CO 2 adsorption and desorption performance of waste ion-exchange resin-based activated carbon

Article *in* Environmental Progress & Sustainable Energy · September 2017

DOI: 10.1002/ep.12743

CITATIONS
3

READS
121

6 authors, including:

Mengqi Wei
Northeastern University (Shenyang, China)
13 PUBLICATIONS **61** CITATIONS
SEE PROFILE

Qingbo Yu
Northeastern University (Shenyang, China)
190 PUBLICATIONS **1,461** CITATIONS
SEE PROFILE

Wenjun Duan
Northeastern University (Shenyang, China)
63 PUBLICATIONS **602** CITATIONS
SEE PROFILE

Zongliang Zuo
Northeastern University (Shenyang, China)
37 PUBLICATIONS **352** CITATIONS
SEE PROFILE

AIChE

CO_2 Adsorption and Desorption Performance of Waste Ion-Exchange Resin-Based Activated Carbon

Mengqi Wei, Qingbo Yu, Wenjun Duan, Zongliang Zuo, Limin Hou, and Jinjie Dai

School of Metallurgy, Northeastern University, No 11, Lane 3, Wenhua Road, Heping District, Shenyang, Liaoning 110819, The People's Republic of China; yuqb@smm.neu.edu.cn (for correspondence)

Published online 00 Month 2017 in Wiley Online Library (wileyonlinelibrary.com). DOI 10.1002/ep.12743

Activated carbons were produced using waste ion-exchange resin, and the effects of different activation temperatures were researched in this article. The experimental results indicate that the activated carbons are microporous carbons. The BET specific surface area and total volume increase at first and then decrease as the activation temperature increases. The maximum adsorption capacity is 81.24 mg/g at 30°C. A higher adsorption temperature and lower CO_2 partial pressure resulted in a lower CO_2 adsorption capacity. After 20 adsorption–desorption cycles, the CO_2 adsorption capacity decreases slightly, and the regeneration degree is always at a high level, which indicates that the activated carbons can be used for a long time. The results in this work suggest that waste ion-exchange resin-based activated carbons show great potential as adsorbents for post-combustion CO_2 capture. © 2017 American Institute of Chemical Engineers Environ Prog, 00: 000–000, 2017

Keywords: waste ion-exchange resin, activated carbon, carbon dioxide, adsorption, desorption

INTRODUCTION

Global warming caused by greenhouse gases is regarded as a very serious challenge for the sustainable development of humans. Carbon capture and storage (CCS) is a method to reduce CO_2 emissions to mitigate global warming. Among CCS technologies, adsorption has been developed and has received attention from researchers owing to the many alternative adsorbents, low cost of the equipment and operation, ease of automation, and the high-purity product obtained [1]. However, the performance of adsorption is poor for the treatment of large emission volumes, and its separation efficiency is also poor [2]. Despite these drawbacks, adsorption is still considered a promising technology, as it offers potential energy savings compared to absorbent systems [3]. The biggest obstacle to applying CCS is the high cost. The capture cost of CCS is approximately 75% of the total cost [4], so reducing the capture cost is particularly important. For adsorption, there are three ways to reduce the cost: first, reduce the adsorbent cost; second, increase the adsorption capacity of the adsorbent; third, improve the adsorption–desorption process cycle.

The common adsorbents used to separate CO_2 from flue gas are porous carbonaceous materials [5–7], metal oxides [8,9], zeolites [10,11], mesoporous silicas [10,12], and metal organic frameworks (MOFs) [13,14] at present. Activated carbon (AC), which is one type of carbonaceous material, is used for CO_2 capture because of its alternative precursors, high surface area, environmental friendliness, low cost, excellent thermal stability, special surface properties, and ability to operate in a wide temperature and pressure range [15,16].

Ion-exchange resins have been applied widely to the fields of industrial high purity water preparation, health and medicine, metallurgical industry, bioengineering, etc. After several uses, the performance of the resin will degrade, and it will be discarded. Waste ion-exchange resin (WIR) is a solid hazardous waste, and its disposal is a problem. The large amounts of WIR cannot be disposed of quickly, which has become a severe problem for WIR users. WIR was found to be a suitable precursor to produce ACs. WIR has been discarded as waste, so using it to prepare ACs turns waste into wealth, solves the terminal disposal problem of WIR and reduces the cost of ACs. Based on the present papers, WIR use for producing ACs may have potential economic and ecological advantages. ACs produced by WIR have been used for sewage treatment [17,18], naphthalene adsorption [19], and high-performance supercapacitors [20], but no one has used the ACs to separate CO_2 from flue gas as far as we know.

In this article, to reduce the cost of CO_2 emissions, the first method (reduction of the adsorbent cost) was chosen, so WIR was used as a precursor to produce ACs as a low-priced adsorbent. Then, the ACs were applied to CO_2 adsorption. The CO_2 adsorption, desorption, and cycling performances of the ACs were investigated.

EXPERIMENTAL

Preparation of the ACs

The WIR (a type of cation exchange resin designated D001 according to the Ministerial standard of petroleum chemical industry of the People's Republic of China, 1978) was pretreated with 5% HCl, washed with distilled water, and then dried in a drying oven. The treated WIR was heated to 800°C at a rate of 5°C/min and kept at that temperature for 60 min under a N_2 atmosphere.

Char and KOH were mixed (the ratio of KOH to char was 1.5) and heated from room temperature to the required activation temperature for 2 h at a rate of 5°C/min in an atmosphere of N_2. After cooling to the ambient temperature, the WIR-based activated carbons (WIRACs) were washed with distilled water until the pH value was approximately 7, and then, they were dried in a drying oven overnight.

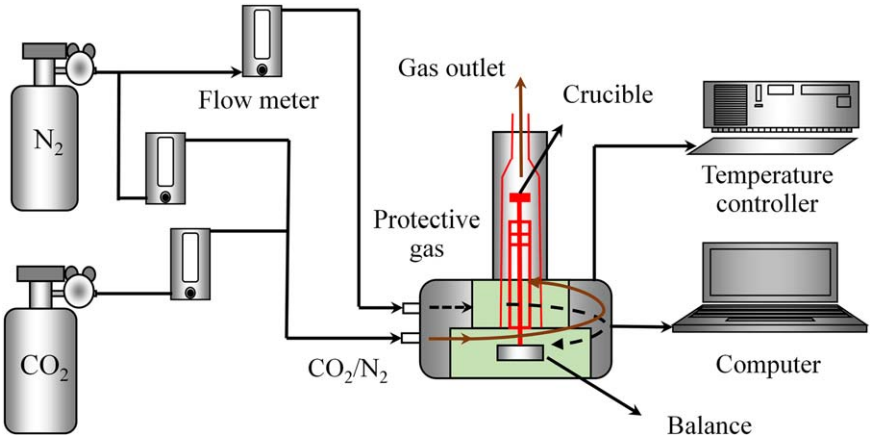

Figure 1. Experimental procedure diagram of TGA. [Color figure can be viewed at **wileyonlinelibrary.com**]

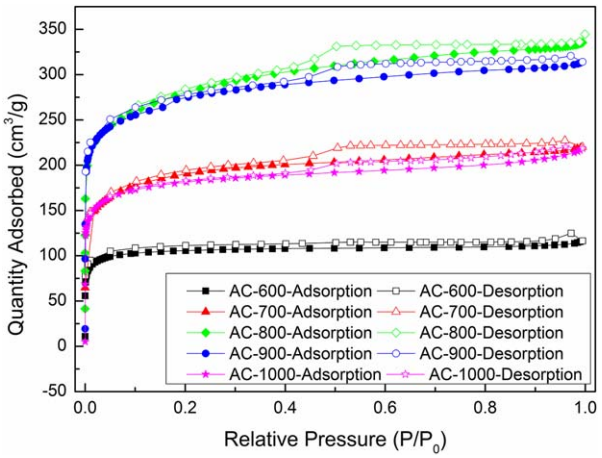

Figure 2. N_2 adsorption–desorption isotherms of WIRACs. [Color figure can be viewed at **wileyonlinelibrary.com**]

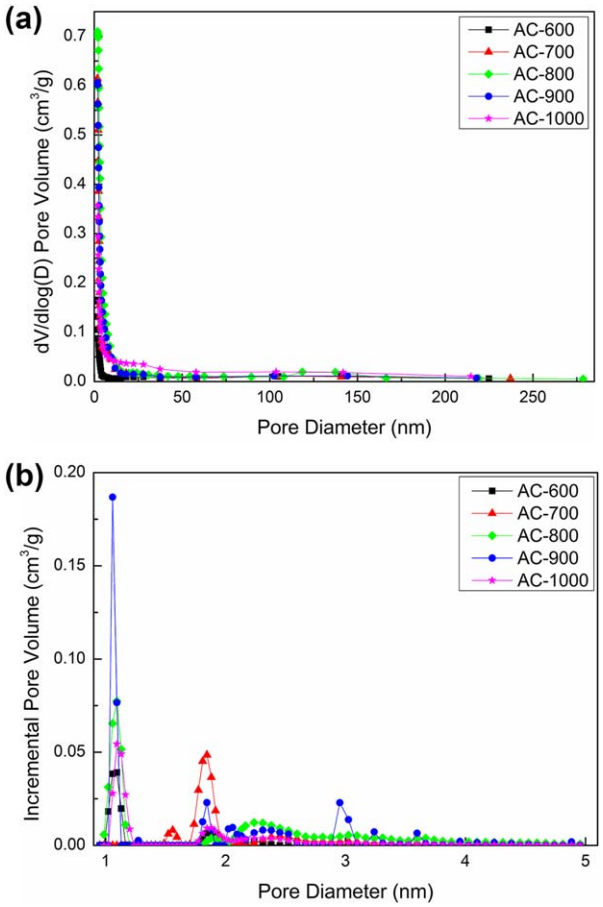

Figure 3. Pore size distributions of WIRACs: (a) BJH model; and (b) DFT model. [Color figure can be viewed at **wileyonlinelibrary.com**]

Textural Characterization of the WIRACs

The N_2 adsorption–desorption isotherms of the WIRACs at −196°C were tested using a specific surface area and pore size analyser (TriStar II 3020, Micromeritics Instrument Corporation). The BET equation was used to calculate the specific surface area (S_{BET}). The micropore areas (S_{mic}), and micropore volumes (V_{mic}) were calculated using the D-R equation. The total pore volumes (V_{total}) were acquired at the relative pressure of P/P_0=0.995. Pore size distributions were obtained by applying the BJH and DFT models.

The WIRACs were ground and mixed with KBr at a mass ratio of 1:100 and then ground together into powders. Then, 151.5 mg of the mixed powders was pressed into a slice and subjected to Fourier transform infrared spectroscopy (FTIR) scans (Varian 600-IR, Agilent Technologies). Thirty-two scans were taken in a wavenumber range of 400–4000 cm^{-1} with a resolution of 4 cm^{-1}.

The morphologies of the WIRACs before and after the CO_2 adsorption were obtained using scanning electron microscopy (SEM) (Ultra Plus, Carl Zeiss AG).

Carbon Dioxide Adsorption Capacity

The CO_2 adsorption capacities of the WIRACs were tested using a TGA (STA409PC, Netzsch) at atmospheric pressure, and the experimental procedure diagram can be seen in Figure 1. Approximately 10 mg of the WIRACs was placed in the TGA and heated to 120°C under a N_2 atmosphere to remove CO_2, H_2O and some other impurities adsorbed on the surface of the WIRACs before the adsorption experiment. When the temperature decreased to the required temperature, the N_2 was changed to the designated atmosphere, which was maintained for 30 min.

The Desorption and Cycling Performances of the WIRACs

After the adsorption experiment, the WIRACs with adsorbed CO_2 were heated to a designated temperature at a

certain heating rate under a N_2 atmosphere and kept for 30 min at the designed temperature to desorb the CO_2. Then, the WIRACs were used to repeat the previous CO_2 adsorption process.

The regeneration degree is defined as follows:

$$D_{reg} = \frac{m_{reg}}{m_1} \quad (1)$$

where m_{reg} is the CO_2 adsorption capacity of the regenerated WIRACs, and m_1 is the CO_2 adsorption capacity of the fresh WIRACs. The regeneration degree represents whether the adsorbent regeneration was easy or hard; and the closer to the unit the value is, the easier it is to regenerate the adsorbent.

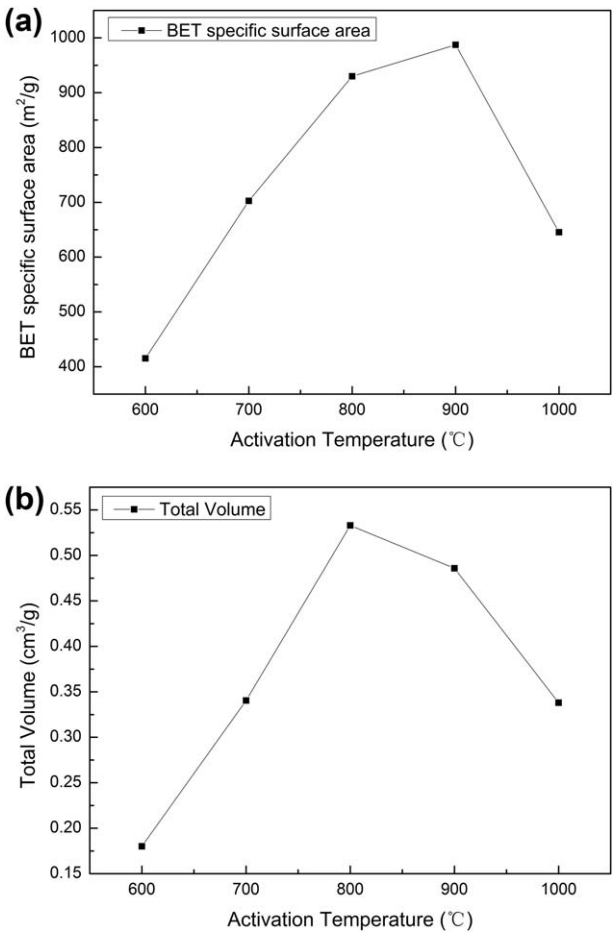

Figure 4. Effect of activation temperature on pore structure: (a) BET specific surface area; and (b) total volume.

RESULTS AND DISCUSSION

Textural Characterization

Adsorption Isotherms and Pore Size Distributions

Figure 2 illustrates the N_2 adsorption–desorption isotherms of the WIRACs. At a very low relative pressure (P/P_0<0.03), the N_2 adsorption amounts increase rapidly. When the relative pressure is higher than 0.1, the adsorption amounts increase slightly as the relative pressure increases. After the adsorption amounts reach saturation, the adsorption isotherms show slight up-tilted tails. According to the IUPAC adsorption isotherm classification [21], the WIRACs present type I N_2 adsorption isotherms. The hysteresis loops show a slit shape in the horizontal direction. Based on the IUPAC adsorption hysteresis loops [22], the WIRACs present an H4 hysteresis loop, which is caused by atypical slit-like pores.

Figure 3 shows the pore size distributions using the BJH and DFT models. As shown in Figure 3a, the pore sizes of the WIRACs indicate micropores and some mesopores. Therefore, a DFT model was used to analyze the pore size distributions. As shown in Figure 3b, the pore sizes of the WIRACs have multipeak distributions. The pore sizes are in the range of 0.9–4 nm, especially 0.9–2.5 nm, which is good for small molecule adsorption. The dynamic diameter of CO_2 is 0.33 nm, indicating that the pore range of the WIRACs is suitable for CO_2 adsorption.

Effect of the Activation Temperature on the Pore Structure and Yield

The effect of the activation temperatures was tested in the range of 600°C to 1000°C, and the results are presented in Figure 4, which shows that as the activation temperature increases, the BET specific surface area increases at first and then decreases. The total volume is the same as the variation of the BET specific surface area, increasing at first and then

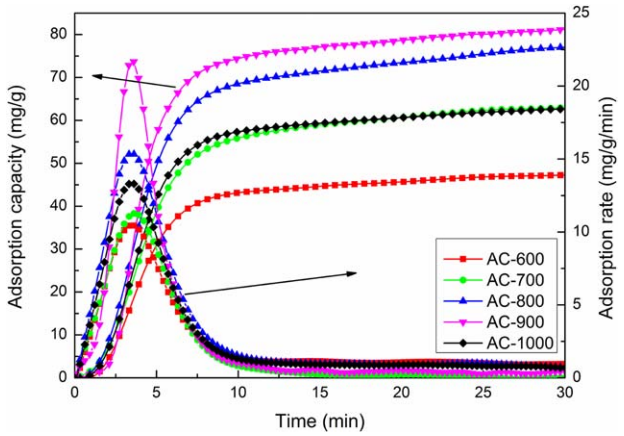

Figure 5. CO_2 adsorption of WIRACs at 30°C and pure CO_2. [Color figure can be viewed at **wileyonlinelibrary.com**]

Table 1. Pore structure parameters, yield, CO_2 adsorption capacity and heat of adsorption of WIRACs.

Sample	S_{BET} (m^2/g)	S_{mic} (m^2/g)	V_{mic} (cm^3/g)	V_{total} (cm^3/g)	D_{ave} (nm)	Yield (%)	CO_2 adsorption capacity (mg/g)	Heat of adsorption (kJ/mol)
AC-600	415	228	0.108	0.180	1.74	38.10	47.26	15.90
AC-700	703	274	0.202	0.340	1.94	33.33	62.99	21.96
AC-800	930	532	0.274	0.533	2.29	29.81	77.04	21.23
AC-900	987	554	0.259	0.486	1.97	24.89	81.22	18.20
AC-1000	645	383	0.171	0.338	2.09	19.75	62.62	16.42

Table 2. The adsorption capacity of CO_2 by ACs in different literatures.

Sample	Adsorption capacity	Experimental conditions and equipment	References
AC-900	81.22 mg/g	30°C, 100% CO_2, 1bar; TGA	This article
AC1	0.75 wt % (7.5 mg/g)	RT, 1bar; IGA	Ref. 26
	3.30 wt % (33 mg/g)	RT, 20bar; IGA	
AC4–200-400He	8.19 wt % (81.9 mg/g)	RT, 1bar; IGA	
	22.38 wt % (223.8 mg/g)	RT, 20bar; IGA	
A	6.9 wt % (69 mg/g)	25°C, 100% CO_2, 1bar; TGA	Ref. 27
AA750	11.7 wt % (117 mg/g)		
AC	2.1mmol/g (92.4 mg/g)	298K, 1bar; IGA	Ref. 28
NPC10	3.2 mmol/g (140.8 mg/g)	298K, 1bar; IGA	
C-700	0.8 mmol/g (35.3 mg/g)	30°C, 100% CO_2, TGA	Ref. 29
MF-700	1.29 mmol/g (56.76 mg/g)	30°C, 100% CO_2, ASAP 2010	Ref. 30
C@MF-*x*	3.4–4.3 mmol/g (149.6–189.2 mg/g)	20°C, 100% CO_2, 760 mmHg, Quantachrome Autosorb-1MP	Ref. 31

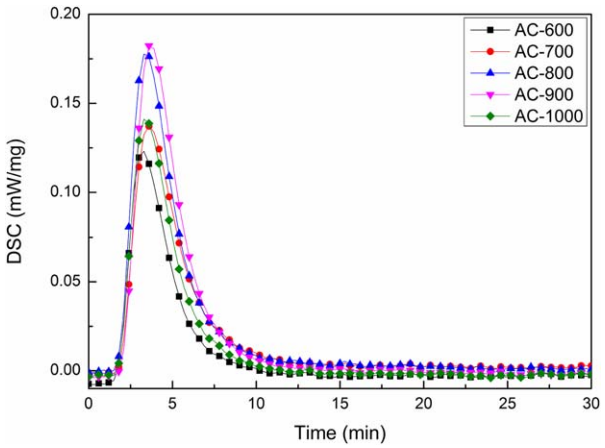

Figure 6. The DSC curves of CO_2 adsorption. [Color figure can be viewed at **wileyonlinelibrary.com**]

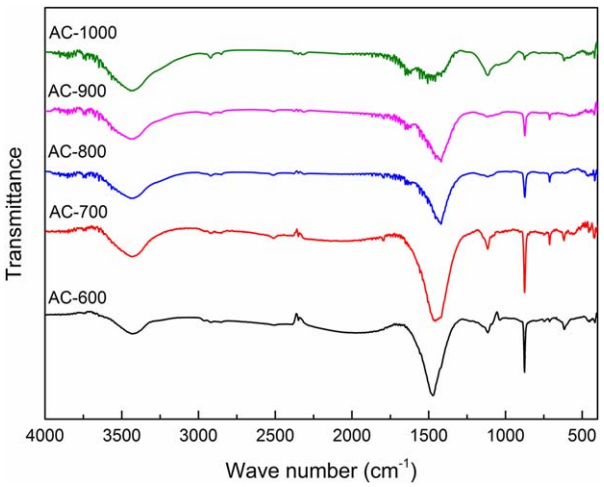

Figure 7. Representative FTIR spectra of different WIRACs. [Color figure can be viewed at **wileyonlinelibrary.com**]

decreasing. The BET specific surface area reaches its maximum at 900°C, while the total volume reaches its maximum at 800°C. When the temperature is low, only a few carbon atoms can react with KOH, and the activation reaction is influenced by the amount of the active atoms, and only a few micropores form. As the temperature increases, more carbon atoms can react with KOH, and more micropores and mesopores form. As reported in the literature, alkali metal atoms are removed from the intercalated system at higher temperatures, forming pores, and the surface area and total volume increase [23]. When the activation temperature is too high, the formed micropores and mesopores are burned off, and the carbon matrix collapses and blocks the pores. Hence, both the BET specific surface area and the total volume decrease. An excessive activation temperature is not advantageous for the activation reaction.

The yield of the WIRACs can be seen in Table 1. Table 1 demonstrates that as the temperature increases, the yield continuously decreases. The char reacts with KOH, and CO_2, CO, and H_2 can be given off in the activation process [24,25]. With an increase in activation temperature, the activation reaction gradually intensifies. Therefore, the amount of the end WIRACs reduces because more char is burned off and more gases are given off.

CO_2 Adsorption Capacity of WIRACs

The CO_2 adsorption capacity of the WIRACs was tested at 30°C with pure CO_2. Figure 5 illustrates the CO_2 adsorption capacity and rate of the WIRACs. The adsorption capacity increases at first and then decreases as the activation temperature increases. The maximum adsorption capacity is 81.22 mg/g when the activation temperature is 900°C. The adsorption capacity is near saturation at approximately 13 min; after 13 min, although the adsorption amount increases, the percentage of the adsorption capacity is not large. The adsorption rate increases at first, then decreases, and finally reaches a constant approaching 0 as the adsorption progresses.

The CO_2 adsorption of the WIRACs occurs on the surface or the interspace of the micropores. First, the CO_2 molecules diffuse from the gas bulk to the outer surface of the WIRAC particles via an imaginary fluid interface membrane on the surface of the WIRACs. Next, the CO_2 molecules migrate from the outer surface of the particles to the inner surface, and finally, the CO_2 molecules are adsorbed by the adsorption sites on the inner surface of the WIRACs. In the beginning, the adsorption capacity increases slowly, indicating the hysteresis phenomenon exists in the adsorption process. In addition, the hysteresis phenomenon is caused by the CO_2 molecules diffusing from the gas bulk to the pores.

The CO_2 adsorption capacity of the WIRACs was compared with some other ACs. In addition, the comparison results can be seen in Table 2. As shown in Table 2, the adsorption capacity of the WIRACs is in the middle level. In addition, when considering the precursor of the WIRACs,

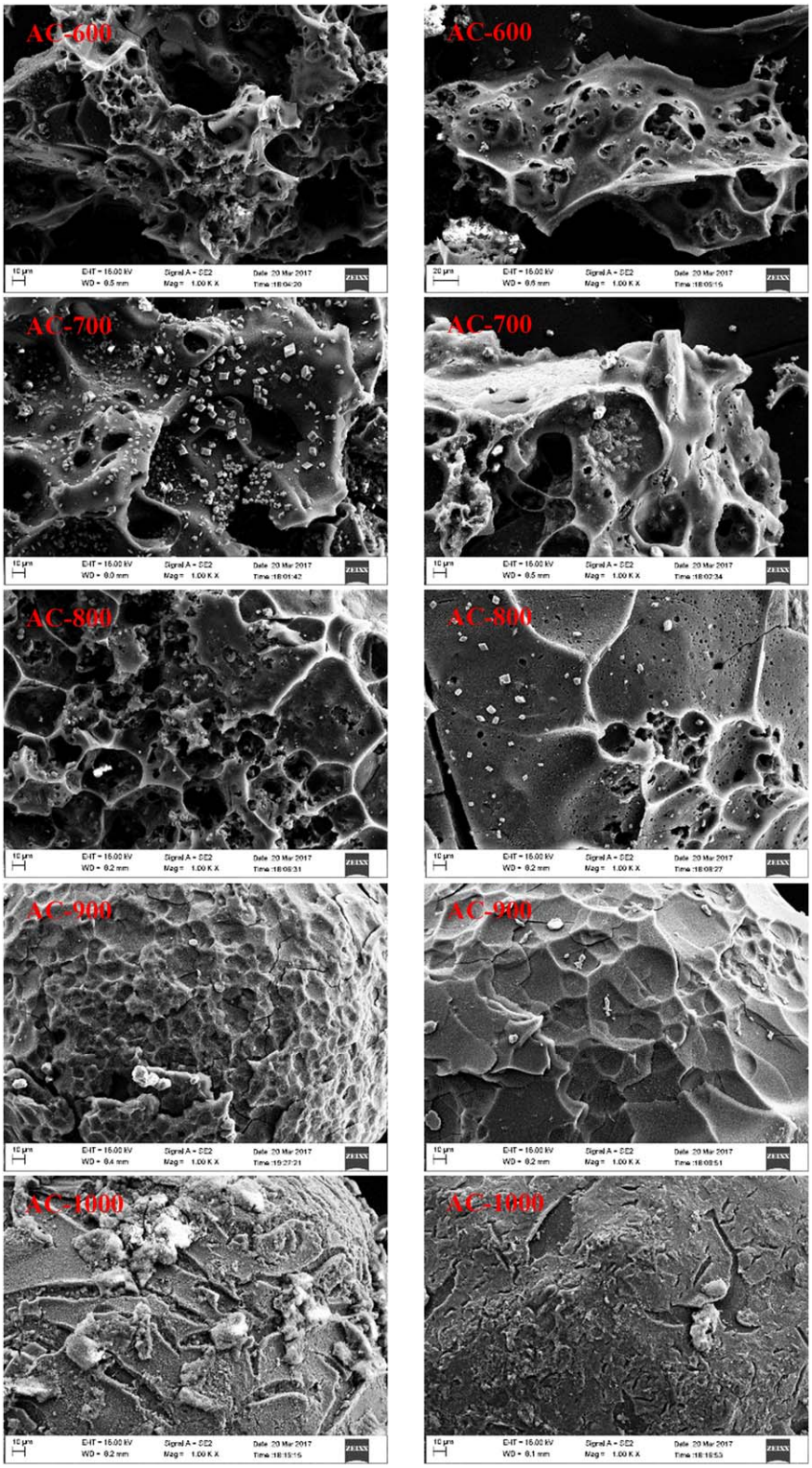

Figure 8. The SEM micrographs of different WIRACs before and after CO_2 adsorption ×1000 (The left is before CO_2 adsorption; the right is after). [Color figure can be viewed at **wileyonlinelibrary.com**]

WIRACs show great potential as adsorbents for postcombustion CO_2 capture.

Figure 6 is the DSC curves of CO_2 adsorption on different WIRACs. As shown in Figure 6, the time of the exothermic process is approximately 13 min, which is consistent with an adsorption process. From the DSC curves, the mass and CO_2 adsorption capacity and the heat of adsorption of the WIRACs can be calculated. The heat of adsorption can be seen in Table 1. The heat of adsorption values range from 15.90 to 21.96 kJ/mol. The enthalpy value for physisorption is

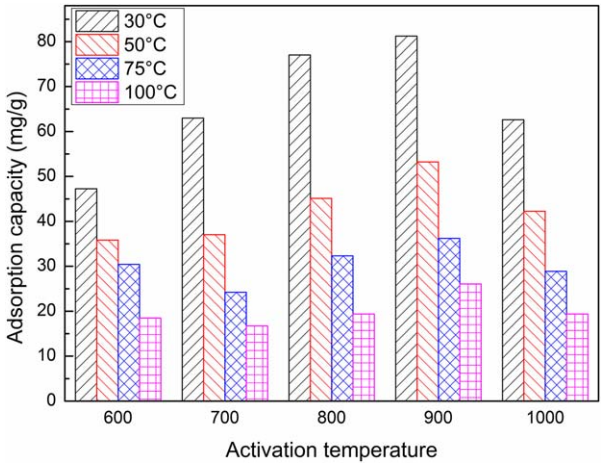

Figure 9. CO_2 adsorption capacity at different temperatures. [Color figure can be viewed at **wileyonlinelibrary.com**]

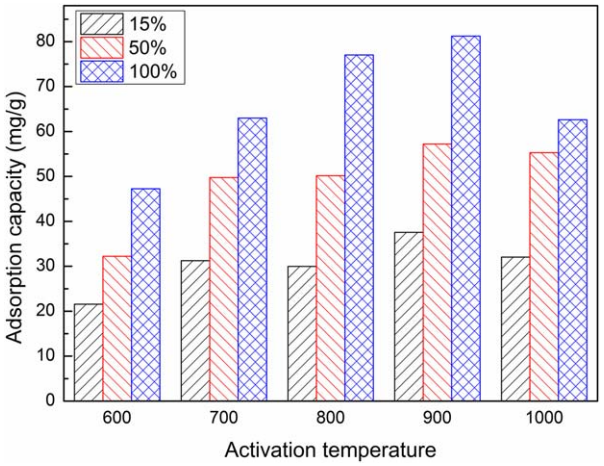

Figure 10. CO_2 adsorption capacity at different CO_2 partial pressures. [Color figure can be viewed at **wileyonlinelibrary.com**]

lower than 20 kJ/mol, while the chemisorption value is in the range of 80–200 kJ/mol [32,33]. The obtained heat of adsorption amounts for all the WIRACs are smaller than 80 kJ/mol, which shows that the CO_2 adsorption is dominated by physical adsorption.

To research the nature of the surface functional groups present on the surface of the WIRACs, an FTIR analysis was performed. The representative FTIR spectra of different WIRACs can be seen in Figure 7. As shown in Figure 7, three main peaks were observed in the spectra of the five WIRACs. The O-H stretching vibration in water exists in the range of 3450–3442 cm^{-1}. The peak at 1550–1400 cm^{-1} is attributed to the —N═N— stretching vibration in azo compounds. The band at 980–780 cm^{-1} is related to CH deformation in aldehydes. The other peaks can be more or less seen in the spectra. The C—O stretching vibration in alcohols exists in the range of 1125–1090 cm^{-1}. The peak at 730–650 cm^{-1} is attributed to CH deformation in alkenes. The band at 700–600 cm^{-1} is related to the S—C stretching vibration in sulfur compounds. According to the spectra, there is only one peak for a nitrogen-containing group, named —N═N—. Because of the few nitrogen-containing groups on the surface of the WIRACs, the CO_2 adsorption capacity is mainly because of physical adsorption based on the pore structure of the WIRACs. The result is the same as the heat of adsorption analysis result.

Figure 8 shows the SEM micrographs of different WIRACs before and after CO_2 adsorption. As shown in Figure 8 in the left five graphs, the macropores or mesopores can be seen clearly on the surface of AC-600, AC-700, and AC-800, while those on AC-900 and AC-1000 cannot be seen. That is, the micropores of AC-600, AC-700, and AC-800 are smaller than those on AC-900 and AC-1000, which corresponds to the pore structure results. Comparing the left and right graphs, before and after CO_2 adsorption, shows that the morphologies of the WIRACs were virtually unchanged.

The CO_2 adsorption capacity of the WIRACs was tested at different adsorption temperatures and CO_2 partial pressures. Figure 9 illustrates the CO_2 adsorption capacity at different adsorption temperatures. The CO_2 adsorption capacity decreases as the adsorption temperature increases.

Physical adsorption is a spontaneous reaction, so the Gibbs free energy, ΔG, is negative. When physical adsorption occurs, the adsorbates migrate from the gas bulk to the adsorption sites, and the degree of freedom (disorder degree) of the gas molecules reduces by at least one dimension, leading to the entropy of the system reducing. In other words, the ΔS of the system is less than zero. Owing to the basic thermodynamics relation formula:

$$\Delta H = \Delta G + T\Delta S \tag{2}$$

when physical adsorption occurs, the adsorption enthalpy of the system (ΔH) must be negative. Hence, physical adsorption is an exothermic reaction. The result agrees with the analysis of the DSC curves.

CO_2 adsorption by WIRACs with their pore structure is a typical physical adsorption, which is an exothermic reaction. As the adsorption temperature increases, the exothermic reaction will be inhibited, which is not conducive to the reaction. For physical adsorption, the adsorption capacity decreases as the adsorption temperature increases. That means a high temperature is not advantageous for CO_2 adsorption. However, for practical applications, flue gas after waste heat recovery is not at room temperature. The temperature of the flue gas is approximately 50–80°C after desulfurization in the power plant. In that temperature range, the CO_2 adsorption capacity of the WIRACs is lower than that at room temperature. In response to this issue, there are two ways to solve this problem. One is to continue reducing the temperature of the flue gas, and the other is to improve the adsorption capacity of WIRACs in a higher temperature range.

Figure 10 shows the CO_2 adsorption capacity at different CO_2 partial pressures. The CO_2 adsorption capacity reduces as the CO_2 partial pressure decreases. The gas molecule dynamic diameters of CO_2 and N_2 are similar (CO_2 is 0.33 nm, and N_2 is 0.364 nm). N_2 will interfere with CO_2 while the WIRACs adsorb CO_2. When the CO_2 partial pressure is low, CO_2 dilution by N_2 makes the CO_2 adsorption by the WIRACs difficult. Additionally, some of the adsorbed CO_2 molecules are purged by more N_2, which desorbs some CO_2.

CO_2 adsorption can be represented as the following reaction:

$$CO_2(g) + AC(s) \rightleftharpoons (AC) \cdot (CO_2)(s) \tag{3}$$

The reaction is a typical gas–solid reaction. In addition, the pressure of the system decreases gradually as the reaction progresses. Increasing the reactant partial pressure (CO_2 partial pressure) or total pressure of the flue gas is advantageous for CO_2 adsorption.

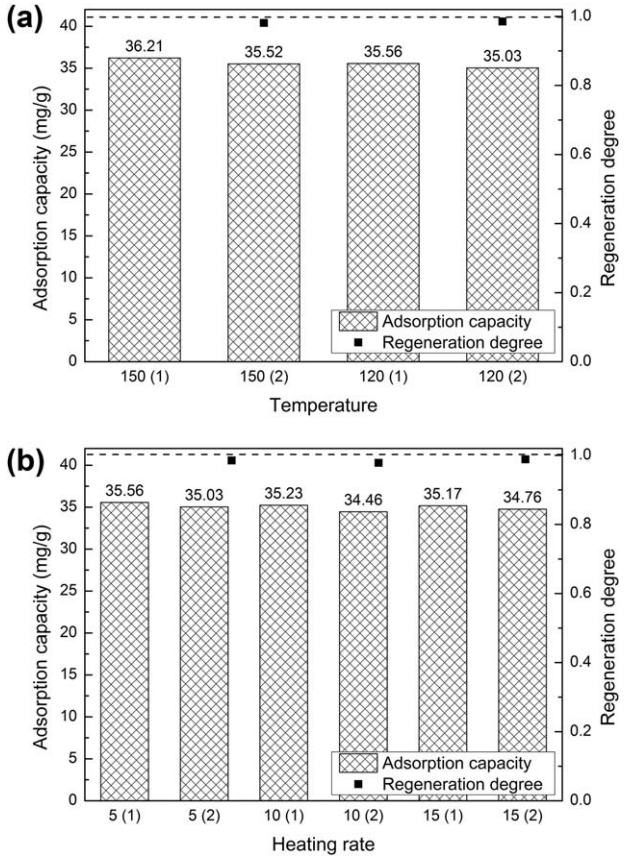

Figure 11. Different desorption conditions and regeneration degree of WIRACs: (a) different temperatures at 5°C/min; and (b) different heating rates at 120°C.

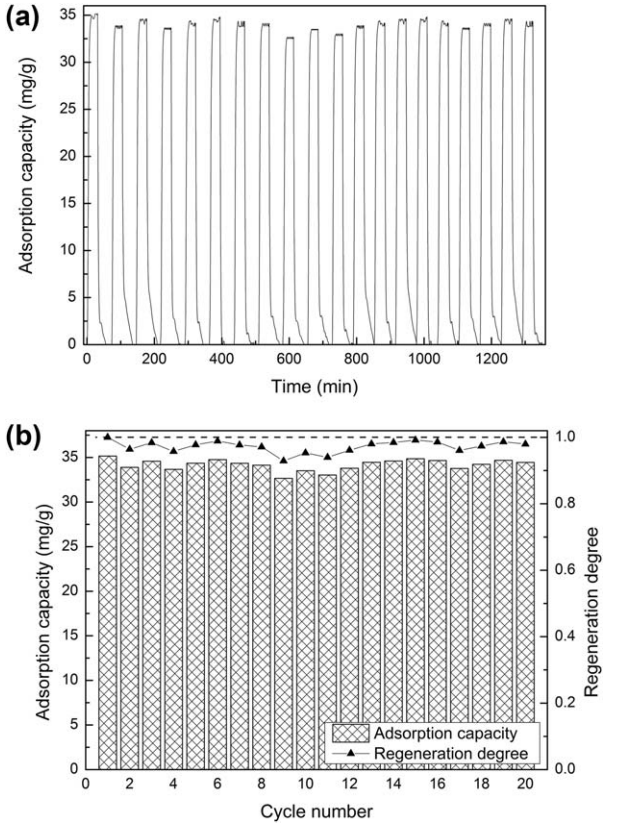

Figure 12. Cyclic CO_2 adsorption on WIRACs via thermal desorption: (a) adsorption curve; and (b) adsorption capacity and regeneration degree.

The CO_2 concentration in the flue gas of a power plant is approximately 15%. Most of the flue gas is composed of N_2, a little water, and other impurities (NO_x, SO_2), which means the CO_2 partial pressure is low. In this case, there are three ways to improve the CO_2 adsorption capacity by either improving the CO_2 concentration, increasing the total pressure of the flue gas, or improving the CO_2/N_2 selectivity of the adsorbents.

CO_2 Desorption and Cycling Performances

As the reverse process of adsorption, desorption is an important part of CO_2 capture. After CO_2 adsorption, the WIRACs need to regenerate via CO_2 desorption. There are two ways to regenerate an adsorbent: reducing the pressure or increasing the temperature, i.e., pressure swing adsorption or temperature swing adsorption, respectively.

The AC-900 WIRAC was chosen to test the desorption properties. The adsorption conditions were 75°C and 100% CO_2. The adsorption experiments were the same as in the previous part. The desorption temperatures were 120°C and 150°C, and the heating rate was 5°C/min. As shown in Figure 11a, 150°C and 120°C were tested as the CO_2 desorption temperatures. The desorption properties of 150°C and 120°C are both good. The CO_2 adsorption capacity of the WIRACs changes some after the first desorption. The regeneration degrees are 0.9809 and 0.9851, respectively. When the desorption temperature is 120°C, the regeneration degree is over 0.98. Therefore, it is unnecessary to further increase the temperature for CO_2 desorption. In addition, in the following experiment, 120°C was chosen as the desorption temperature to test the heating rate. As revealed in Figure 11b, the different heating rates have little effect on the regeneration degree at the same desorption temperature. After the first desorption, the CO_2 adsorption capacity only slightly decreases. The heating rate should be as high as possible when the desorption occurs. If this is so, in a certain process of adsorption–desorption cycles, the number of cycles will increase, while the desorption time is shortened, which will indirectly improve the CO_2 adsorption capacity.

In the cycling process, the desorption temperature and heating rate were 120°C and 15°C/min, respectively. Figure 12 shows the CO_2 adsorption capacity and regeneration degree at 75°C under pure CO_2 conditions. It is clear that CO_2 can be effectively desorbed from the WIRACs during the 20 cycles. In other words, the stability of the WIRACs is high, which is advantageous for practical applications.

CONCLUSIONS

WIRACs derived from WIR were applied to CO_2 adsorption for the first time. The produced WIRACs are microporous carbons, which are suitable for CO_2 adsorption. The BET specific surface area and total volume increase at first and then decrease as the activation temperature increases. An excessive activation temperature, which is not advantageous for the pore structure, can destroy the formed pores, leading to a carbon matrix collapse. The maximum CO_2 adsorption capacity is 81.24 mg/g at 30°C under pure CO_2 conditions. A higher temperature and lower CO_2 partial pressure should be avoided in practical applications because higher adsorption temperatures and lower CO_2 partial pressures are detrimental to CO_2 adsorption. When the temperature is 120°C, the regeneration degree is good, and the different heating rates have little effect on the regeneration degree. After 20 cycles, the CO_2 adsorption capacity

decreases slightly. However, the stability of the CO_2 adsorption by the WIRACs is good, so the WIRACs can be used for a long time. The WIRACs are a promising porous adsorbent for CO_2 capture. This turns waste into wealth, solves the terminal disposal problem of waste resins and reduces the cost of ACs. Although the CO_2 adsorption capacity of the WIRACs is not very large, using WIRACs for CO_2 adsorption can reduce the cost of capture and be good for the application of CCS technology when considering the low cost of WIRACs. In the following work, the CO_2 adsorption capacity should be improved, and the selectivity of CO_2/N_2 should be further studied to investigate the property of the WIRACs.

ACKNOWLEDGMENTS

This research was supported by The National Natural Science Foundation of China (51576035), and The National Postdoctoral Program for Innovative Talents (BX201600028).

LITERATURE CITED

1. Wang, Q.A., Luo, J.Z., Zhong, Z.Y., & Borgna, A. (2011). CO_2 capture by solid adsorbents and their applications current status and new trends, Energy and Environmental Science, 4, 42–55.
2. Lee, S.Y., & Park, S.J. (2014). A review on solid adsorbents for carbon dioxide capture, Journal of Industrial and Engineering Chemistry, 23, 1–11.
3. Martín, C.F., Plaza, M.G., García, S., Pis, J.J., Rubiera, F., & Pevida, C. (2011). Microporous phenol–formaldehyde resin-based adsorbents for pre-combustion CO_2 capture, Fuel, 90, 2064–2072.
4. Plasynski, S.I., Litynski, J.T., Mcllvried, H.G., & Srivastava, R.D. (2009). Progress and new developments in carbon capture and storage, Critical Reviews in Plant Sciences, 28, 123–138.
5. Alcañiz-Monge, J., Marco-Lozar, J.P., & Lillo-Ródenas, M.Á. (2011). CO_2 separation by carbon molecular sieve monoliths prepared from nitrated coal tar pitch, Fuel Processing Technology, 92, 915–919.
6. Chen, C., Kim, J., & Ahn, W. (2012). Efficient carbon dioxide capture over a nitrogen-rich carbon having a hierarchical micro-mesopore structure, Fuel, 95, 360–364.
7. Wang, D.X., Ma, X.L., Sentorun-Shalaby, C., & Song, C.S. (2012). Development of carbon-based "Molecular Basket" sorbent for CO_2 capture, Industrial & Engineering Chemistry Research, 51, 3048–3057.
8. Ozcan, D.C., Ahn, H., & Brandani, S. (2013). Process integration of a Ca-looping carbon capture process in a cement plant, International Journal of Greenhouse Gas Control, 19, 530–540.
9. Kierzkowska, A.M., Poulikakos, L.V., Broda, M., & Müller, C.R. (2013). Synthesis of calcium-based, Al_2O_3-stabilized sorbents for CO_2 capture using a co-precipitation technique, International Journal of Greenhouse Gas Control, 15, 48–54.
10. Samanta, A., Zhao, A., Shimizu, G.K.H., Sarkar, P., & Gupta, R. (2012). Post-combustion CO_2 capture using solid sorbents a review, Industrial & Engineering Chemistry Research, 51, 1438–1463.
11. Zhao, Z.L., Cui, X.Y., Ma, J.H., & Li, R.F. (2007). Adsorption of carbon dioxide on alkali-modified zeolite 13X adsorbents, International Journal of Greenhouse Gas Control, 1, 355–359.
12. Watabe, T., & Yogo, K. (2013). Isotherms and isosteric heats of adsorption for CO_2 in amine-functionalized mesoporous silicas, Separation and Purification Technology, 120, 20–23.
13. Herm, Z.R., Swisher, J.A., Smit, B., Krishna, R., & Long, J.R. (2011). Metal-organic frameworks as adsorbents for hydrogen purification and precombustion carbon dioxide capture, Journal of the American Chemical Society, 133, 5664–5667.
14. Yao, Q.X., Su, J., Cheung, O., Liu, Q.L., Hedin, N., & Zou, X.D. (2012). Interpenetrated metal-organic frameworks and their uptake of CO_2 at relatively low pressures, Journal of Materials Chemistry, 22, 10345–10351.
15. Lee, C.S., Ong, Y.L., Aroua, M.K., & Daud, W.M.A.W. (2013). Impregnation of palm shell-based activated carbon with sterically hindered amines for CO_2 adsorption, Chemical Engineering Journal, 219, 558–564.
16. Mahurin, S.M., Gorka, J., Nelson, K.M., & Mayes, R.T. (2014). Enhanced CO_2/N_2 selectivity in amidoxime-modified porous carbon, Carbon, 67, 457–464.
17. Bratek, K., Bratek, W., & Kułażyński, M. (2002). Carbon adsorbents from waste ion-exchange resin, Carbon, 40, 2213–2220.
18. Gun'ko, V.M., Leboda, R., Skubiszewska-Zięba, J., Charmas, B., & Oleszczuk, P. (2005). Carbon adsorbents from waste ion-exchange resins, Carbon, 43, 1143–1150.
19. Shi, Q.Q., Li, A.M., Zhu, Z.L., & Liu, B. (2013). Adsorption of naphthalene onto a high-surface-area carbon from waste ion exchange resin, Journal of Environmental Sciences China, 25, 188–194.
20. Zhang, Z.J., Cui, P., Chen, X.Y., & Liu, J.W. (2013). The production of activated carbon from cation exchange resin for high-performance supercapacitor, Journal of Solid State Electrochemistry, 17, 1749–1758.
21. Brunauer, S., Deming, L.S., Deming, W.E., & Teller, E. (1940). On a theory of the van der Waals adsorption of gases, Journal of the American Chemical Society, 62, 1723–1732.
22. Sing, K.S.W., Everett, D.H., Haul, R.A.W., Moscou, L., Pierotti, R.A., Rouquérol, J., & Siemieniewska, T. (1985). Reporting physisorption data for gas solid systems with special reference to the determination of surface area and porosity, Pure and Applied Chemistry, 54, 603–619.
23. Gurten, I.I., Ozmak, M., Yagmur, E., & Aktas, Z. (2012). Preparation and characterisation of activated carbon from waste tea using K_2CO_3, Biomass and Bioenergy, 37, 73–81.
24. Martinez-Escandell, M., de Castro, M.M., Molina-Sabio, M., & Rodriguez-Reinoso, F. (2013). KOH activation of carbon materials obtained from the pyrolysis of ethylene tar at different temperatures, Fuel Processing Technology, 106, 402–407.
25. Song, M., Jin, B.S., Xiao, R., Yang, L., Wu, Y.M., Zhong, Z.P., & Huang, Y.J. (2013). The comparison of two activation techniques to prepare activated carbon from corn cob, Biomass and Bioenergy, 48, 250–256.
26. Caglayan, B.S., & Aksoylu, A.E. (2013). CO_2 adsorption on chemically modified activated carbon, Journal of Hazardous Materials, 252, 19–28.
27. Plaza, M.G., Pevida, C., Martin, C.F., Fermoso, J., Pis, J.J., & Rubiera, F. (2010). Developing almond shell-derived activated carbons as CO_2 adsorbents, Separation and Purification Technology, 71, 102–106.
28. Yang, H.W., Yuan, Y.Z., & Tsang, S.C.E. (2012). Nitrogen-enriched carbonaceous materials with hierarchical micro-mesopore structures for efficient CO_2 capture, Chemical Engineering Journal, 185, 374–379.
29. Goel, C., Kaur, H., Bhunia, H., & Bajpai, P.K. (2016). Carbon dioxide adsorption on nitrogen enriched carbon adsorbents: Experimental, kinetics, isothermal and thermodynamic studies, Journal of CO2 Utilization, 16, 50–63.

30. Goel, C., Bhunia, H., & Bajpai, P.K. (2017). Prediction of binary gas adsorption of CO_2/N_2 and thermodynamic studies on nitrogen enriched nanostructured carbon adsorbents, Journal of Chemical & Engineering Data, 62, 214–225.
31. Liu, L., Xie, Z.H., Deng, Q.F., Hou, X.X., & Yuan, Z.Y. (2017). One-pot carbonization enrichment of nitrogen in microporous carbon spheres for efficient CO_2 capture, Journal of Materials Chemistry A, 5, 418–425.
32. Zhou, X., Yi, H.H., Tang, X.L., Deng, H., & Liu, H.Y. (2012). Thermodynamics for the adsorption of SO_2, NO and CO_2 from flue gas on activated carbon fiber, Chemical Engineering Journal, 200, 399–404.
33. Heidari, A., Younesi, H., Rashidi, A., & Ghoreyshi, A.A. (2014). Evaluation of CO_2 adsorption with eucalyptus wood based activated carbon modified by ammonia solution through heat treatment, Chemical Engineering Journal, 254, 503–513.